

Article

Effects of Asymmetric Gas Distribution on the Instability of a Plane Power-Law Liquid Jet

Jin-Peng Guo ^{1,†} , Yi-Bo Wang ^{2,†}, Fu-Qiang Bai ³, Fan Zhang ¹ and Qing Du ^{1,*}

¹ State Key Laboratory of Engines, Tianjin University, Tianjin 300072, China; guojinpeng@tju.edu.cn (J.-P.G.); fanzhang_lund@tju.edu.cn (F.Z.)

² Wuxi Weifu High-Technology Co., Ltd., No. 5 Huashan Road, Wuxi 214031, China; wangyb@tju.edu.cn

³ Internal Combustion Engine Research Institute, Tianjin University, Tianjin 300072, China; bbfq@163.com

* Correspondence: duqing@tju.edu.cn; Tel.: + 86-022-2740-4409

† These authors contributed equally to this work.

Received: 17 May 2018; Accepted: 27 June 2018; Published: 16 July 2018



Abstract: As a kind of non-Newtonian fluid with special rheological features, the study of the breakup of power-law liquid jets has drawn more interest due to its extensive engineering applications. This paper investigated the effect of gas media confinement and asymmetry on the instability of power-law plane jets by linear instability analysis. The gas asymmetric conditions mainly result from unequal gas media thickness and aerodynamic forces on both sides of a liquid jet. The results show a limited gas space will strengthen the interaction between gas and liquid and destabilize the power-law liquid jet. Power-law fluid is easier to disintegrate into droplets in asymmetric gas medium than that in the symmetric case. The aerodynamic asymmetry destabilizes para-sinusoidal mode, whereas stabilizes para-varicose mode. For a large Weber number, the aerodynamic asymmetry plays a more significant role on jet instability compared with boundary asymmetry. The para-sinusoidal mode is always responsible for the jet breakup in the asymmetric gas media. With a larger gas density or higher liquid velocity, the aerodynamic asymmetry could dramatically promote liquid disintegration. Finally, the influence of two asymmetry distributions on the unstable range was analyzed and the critical curves were obtained to distinguish unstable regimes and stable regimes.

Keywords: power-law fluid; instability analysis; asymmetric gas distribution

1. Introduction

The disintegration of plane liquid jets into small droplets plays a significant role on combustion efficiency in numerous applications, such as gas turbines and rocket engines. As a result, a large number of investigations were carried out on the breakup of plane liquid jets, especially for inviscid fluids and Newtonian fluids [1–7].

However, non-Newtonian fluids are also extensively involved in engineering applications, such as coal water slurry [8], gelled propellant [9], and sunflower oil. According to the rheological feature, there exist a lot of types of non-Newtonian fluids, such as viscoelastic fluid, power-law fluid and Bingham fluid. The breakup mechanism of plane non-Newtonian liquid jets was investigated by Liu [10], Brenn [11], Yang [12,13] and Thompson [14] in details. Liu et al. [10] analyzed the instability of a viscoelastic sheet with two-dimensional disturbances. The results showed that viscoelastic liquid sheets had a higher growth rate than Newtonian liquid sheets both for symmetric and antisymmetric disturbances, resulted from the liquid elasticity. Brenn et al. [11] pointed out that two-dimensional disturbances dominated the instability of viscoelastic plane sheets both for symmetric and antisymmetric disturbances. Yang et al. [12] investigated the instability of planar viscoelastic liquid sheets with two gas streams which were subject to unequal velocities. It was found that larger

velocity differences across the interface enhanced sheet instability. Thompson and Rothstein [14] studied the atomization characteristic of viscoelastic fluids ejected from flat-fan and hollow-cone nozzles. The results showed that, for water sheets produced by flat-fan nozzles, fluid rims became unstable first and the additional viscoelasticity stabilized the rim, while the internal liquid sheet was simultaneously destabilizing. Yang et al. [13] carried out spatial and temporal analysis of an electrified viscoelastic liquid jet. It was found that larger electrical Euler number and Weber number can change the flow to be convectively unstable. Liu and Lu [15] analyzed the instability of viscoelastic annular liquid jets in a radial electric field. They found that the radial electric field had a dual impact on viscoelastic annular liquid jets in the temporal mode. With the increase of Weber number, the liquid jet was first in absolute instability and then changes to convective instability.

However, compared with viscoelastic fluids, very limited literatures on the breakup of power-law liquid jets were presented so far, due to the nonlinear features of constitutive equations. Chojnacki and Feikema [16] studied the breakup of a power-law liquid sheet formed by the impinging jets. Based on this work, Yang et al. [17] built a modified physical mode to predict the breakup length and critical wave length and the result agreed well with experiment data. Ma et al. [18] investigated the atomization characteristics, i.e., the velocity distribution and the particle distribution of power-law impinging jets based on PDPA and high-speed camera.

Huang et al. [19] studied the instability of power-law liquid films down an inclined plane. The results showed that a larger Reynolds number can promote the jet instability. Yang et al. [9] analyzed the instability of plane power-law sheets with varicose mode. It was found that with the increase of the sheet thickness, surface tension and the power-law exponent, the disturbance growth rate kept decreasing and the sheet instability was damped. Xia et al. [20] and Deng et al. [21] studied the breakup process of plane power-law jets with two disturbance modes. The results demonstrated that para-sinusoidal mode dominated the liquid breakup. Meanwhile, Deng et al. [21] also pointed out that the instability analysis could effectively reveal the breakup feature of power-law fluids in a comparison between experimental results and theoretical predictions.

It should be pointed out that in the above studies, the gas media surrounding the power-law liquid jet are assumed to be unbounded. In fact, the breakup related with liquid combustion usually occurs in a confined environment. Besides, there exist various gas media, such as fuel vapor, fresh air and exhaust gas in the combustion chamber, which will result in an asymmetric distribution of gas media. Furthermore, in a confined gas environment, there even exist some kind of asymmetric distribution of gas media which will have significant effects on the breakup of liquid jets. It is important to investigate the effect of gas asymmetry on the jet instability in order to understand more thoroughly the breakup mechanism of power-law fluids and provide more references for engineering applications of non-Newtonian fluids.

Accordingly, this paper investigates the influence of two asymmetric gas media on the instability of a power-law plane jet by a linear instability analysis. The gas asymmetry is resulted from unequal gas gaps or aerodynamic forces on both sides of a liquid jet into confined gas medium, called as the boundary asymmetry and aerodynamic asymmetry respectively. The effects of two types of gas asymmetric distribution as well as the competition between both are investigated in detail.

2. Instability Analysis

Consider a plane power-law liquid jet of thickness $2h$, density ρ_l , surface tension σ moving at a uniform velocity u_l into two asymmetric confined gas media. The gas densities on two sides of plane liquid jets are ρ_{g1} and ρ_{g2} . The gas thicknesses are b_1^* and b_2^* , respectively. The effect of gravity is reasonably negligible for both liquid and gas media. Based on Li's investigation [4], there are two types of unstable waves on the gas-liquid interfaces which are para-sinusoidal mode and para-varicose mode, when the physical parameters of gas media on both sides are different. The schematic diagrams of the jet configuration are shown in Figure 1.

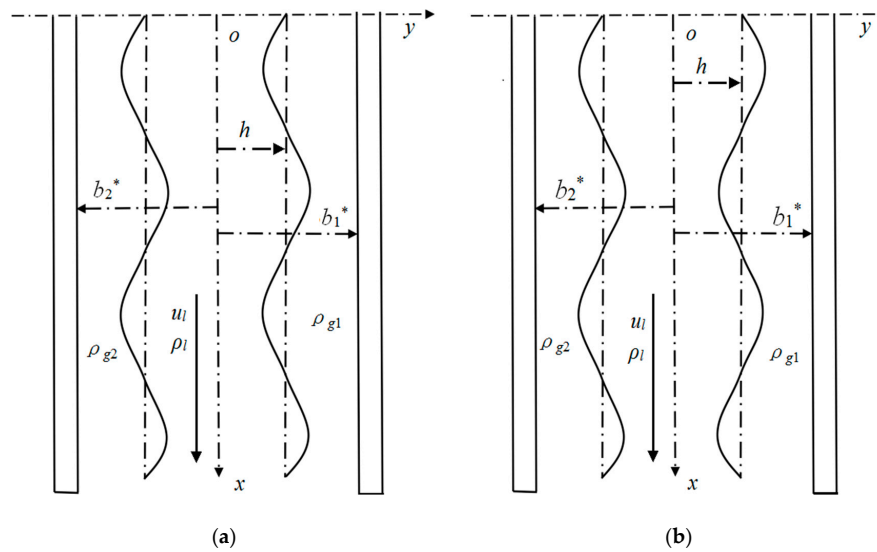


Figure 1. Schematic diagram of a power-law liquid jet in two asymmetric bounded gas media and interface waves: (a) para-sinusoidal mode and (b) para-varicose mode.

Before disturbed, the mean flow field of liquid phase is expressed as follows at $-h \leq y \leq h$:

$$\bar{\mathbf{U}} = (u_l, 0) \quad \bar{P}_l = P_{l0} \tag{1}$$

The mean flow fields of right and left gas phases are separately at $h \leq y \leq b_1^*$ and $-b_2^* \leq y \leq h$:

$$\bar{\mathbf{U}}_{gj} = \mathbf{0} \quad \bar{P}_{gj} = P_{gj0} \tag{2}$$

where, $j = 1$ and 2 represent right and left gas media, respectively.

After a small disturbance is introduced, the gas-liquid interface will leave the balance position and the flow fields of both phases become:

$$\mathbf{u}_l = \bar{\mathbf{u}}_l + \mathbf{u}_l \quad P_l = \bar{P}_l + p_l \tag{3}$$

$$\mathbf{u}_{gj} = \bar{\mathbf{u}}_{gj} + \mathbf{u}_{gj} \quad P_{gj} = \bar{P}_{gj} + p_{gj} \tag{4}$$

For incompressible liquid phase, the equations governing the conservation of mass and momentum in the Cartesian coordinate are expressed:

$$\nabla \cdot \mathbf{u}_l = 0 \tag{5}$$

$$\rho_l \left(\frac{\partial}{\partial t} + \mathbf{u}_l \cdot \nabla \right) \mathbf{u}_l = -\nabla P_l + \nabla \cdot \mathbf{T} \tag{6}$$

where, \mathbf{u}_l is the velocity vector of liquid phase and P_l is the liquid pressure.

The power-law model is used to describe the rheological property of liquid phase:

$$\mathbf{T} = \eta(\dot{\gamma})\dot{\gamma}, \eta(\dot{\gamma}) = K\dot{\gamma}^{n-1}, \dot{\gamma} = \sqrt{\frac{1}{2}tr(\dot{\gamma}^2)} \tag{7}$$

where \mathbf{T} is the extra stress tensor of liquid phase, $\dot{\gamma} = \nabla \mathbf{u} + (\nabla \mathbf{u})^T$ the strain-rate second order symmetric tensor, n the power law exponent, and K the viscosity coefficient.

The non-linear feature of liquid state shows the greatest discrepancy between Newtonian fluids and power-law fluids. It is very difficult to solve the governing equations due to the strong nonlinear viscosity term because of the power-law model, and we have to do some approximation. Besides, in the

actual flow condition of a plane liquid jet, the scale of the disturbance and the jet velocity in the y -axis is very small. So the shear stress τ_{xy} and normal stress τ_{yy} in the y -axis are neglected as reported by Xia et al. [20], Deng et al. [21] and Chang et al. [22]. Then the momentum equations of liquid phase become:

$$\rho_l \left(\frac{\partial U_{lx}}{\partial t} + U_{lx} \frac{\partial U_{lx}}{\partial x} + U_{ly} \frac{\partial U_{lx}}{\partial y} \right) = -\frac{\partial P_l}{\partial x} + \frac{\partial \tau_{xx}}{\partial x} \quad (8)$$

$$\rho_l \left(\frac{\partial U_{ly}}{\partial t} + U_{lx} \frac{\partial U_{ly}}{\partial x} + U_{ly} \frac{\partial U_{ly}}{\partial y} \right) = -\frac{\partial P_l}{\partial y} \quad (9)$$

$$\tau_{xx} = K \left(2 \frac{\partial U_{lx}}{\partial x} \right)^n \quad (10)$$

In order to keep the nonlinear feature, a coefficient g , characterizing the unit change of liquid velocity along x -axis, is introduced to linearize Equation (10). Then, Equation (10) is expanded according to Binomial theorem.

$$\tau_{xx} = K \left(2g + 2 \frac{\partial u_{lx}}{\partial x} \right)^n = K \left[(2g)^n + 2n(2g)^{n-1} \frac{\partial u_{lx}}{\partial x} + \dots \right] \quad (11)$$

Substitute Equations (1) and (11) into Equation (5) and Equations (8)~(9) yields the governing equations of the liquid phase upon linearization:

$$\nabla \cdot \mathbf{u}_l = 0 \quad (12)$$

$$\rho_l \left(\frac{\partial u_{lx}}{\partial t} + u_l \frac{\partial u_{lx}}{\partial x} \right) = -\frac{\partial p_l}{\partial x} + 2n(2g)^{n-1} K \frac{\partial^2 u_{lx}}{\partial x^2} \quad (13)$$

$$\rho_l \left(\frac{\partial u_{ly}}{\partial t} + u_l \frac{\partial u_{ly}}{\partial x} \right) = -\frac{\partial p_l}{\partial y} \quad (14)$$

It is reasonable to neglect the viscous effect for two gas media, and then the disturbed governing equations are rewritten as:

$$\nabla \cdot \mathbf{u}_{gj} = 0 \quad (15)$$

$$\rho_{gj} \frac{\partial \mathbf{u}_{gj}}{\partial t} = -\nabla p_{gj} \quad (16)$$

The disturbed parameters are given in the normal mode as following:

$$[\mathbf{u}_l, \mathbf{u}_{gj}, p_l, p_{gj}, \eta_j] = [\hat{\mathbf{u}}_l, \hat{\mathbf{u}}_{gj}, \hat{p}_l, \hat{p}_{gj}, \eta_{0j}] e^{st+ikx} \quad (17)$$

The system should satisfy the kinematic and dynamic boundary conditions at the gas-liquid interfaces. At $y = \pm h + \eta_j$, the linearized kinematic boundaries are shown as:

$$u_{ly} = \frac{\partial \eta_j}{\partial t} + u_l \frac{\partial \eta_j}{\partial x} \quad (18)$$

$$u_{g^j y} = \frac{\partial \eta_j}{\partial t} \quad (19)$$

The dynamic conditions, after linearization, are expressed at $y = \pm h + \eta_j$ as:

$$p_l - p_{gj} \pm \sigma \frac{\partial^2 \eta_j}{\partial z^2} = 0 \quad (20)$$

Meanwhile, the additional boundary conditions at $y = b_1^*$ and $y = -b_2^*$ are:

$$u_{g1y} = u_{g2y} = 0 \quad (21)$$

After a serial of derivation, the characteristic equation between the complex growth rate s and the wave number k is obtained:

$$\begin{aligned} & \left\{ \frac{\rho_l(s+iku_l)^2}{l} \tanh(lh) + \rho_{gl} \frac{s^2}{k} \coth[k(b_1^* - h)] + \sigma k^2 h^2 \right\} \\ & \times \left\{ \frac{\rho_l(s+iku_l)^2}{l} \coth(lh) + \rho_{gl} \frac{s^2}{k} \coth[k(b_1^* - h)] + \sigma k^2 h^2 \right\} \\ & = \frac{s^2}{k} \left\{ \frac{\rho_l(s+iku_l)^2}{l} \frac{\tanh(lh) + \coth(lh)}{2} + \rho_{g1} \frac{s^2}{k} \coth[k(b_1^* - h)] + \sigma k^2 h^2 \right\} \\ & \times \left\{ \rho_{g1} \coth[k(b_1^* - h)] - \rho_{g2} \coth[k(b_2^* - h)] \right\} \end{aligned} \tag{22}$$

where, $l = [1 + 2n(2g)^{n-1} K k^2 (s + iku_l)^{-1}]^{-0.5} k$

Choose $h, u_l, h/u_l, \rho_l$ and $\rho_l u_l^2$ as the reference scales of length, velocity, time, density and pressure, respectively. The dimensionless dispersion relation characterizing the instability of a plane power-law liquid jet into two asymmetric bounded gas media is given as:

$$\begin{aligned} & \left\{ \frac{(S+im)^2}{L} \tanh(L) + Q_1 \frac{S^2}{m} \coth[m(B_1 - 1)] + \frac{m^2}{We} \right\} \\ & \times \left\{ \frac{(S+im)^2}{L} \coth(L) + Q_1 \frac{S^2}{m} \coth[m(B_1 - 1)] + \frac{m^2}{We} \right\} \\ & = \frac{S^2}{m} \left\{ \frac{(S+im)^2}{L} \frac{\tanh(L) + \coth(L)}{2} + Q_1 \frac{S^2}{m} \coth[m(B_1 - 1)] + \frac{m^2}{We} \right\} \\ & \times \left\{ Q_1 \coth[m(B_1 - 1)] - Q_2 \coth[m(B_2 - 1)] \right\} \end{aligned} \tag{23}$$

where, $S = sh/u_l$ is the dimensionless complex frequency, and its real part S_r indicates the dimensionless growth rate of the disturbance. The other dimensionless parameters are Weber number $We = \rho_l u_l^2 h / \sigma$, the generalized Reynolds number $Re = \rho_l u_l^{2-n} h^n / K$ of liquid phase, the gas-liquid density ratio $Q_j = \rho_{gj} / \rho_l$, the gas thickness $B_j = b_j^* / h$ on each side of the jet, the wave number $m = kh$, the parameters $G = gh/u_l$ and $L = lh = [1 + 2n(2G)^{n-1} Re^{-1} (S + im)^{-1}]^{-0.5} m$ respectively.

In the present study, by adopting the temporal instability analysis, the dispersion equation Equation (23) of plane power-law liquid jets can be numerically solved, and the complex solutions of S can be calculated corresponding to each wavenumber m by specifying jet parameters including We, Re, Q_j, G, B_j and n . After solving Equation (23), a set of feature parameters, both for para-varicose mode disturbance and para-sinuuous mode disturbance, can be obtained to indicate the instability characteristics of power-law liquid jets under different flow conditions.

If $Re \rightarrow \infty, n = 1, Q_1 = Q_2 = Q$ and $B_1 = B_2 = B \rightarrow \infty$, Equation (23) is identical to that of a plane inviscid liquid jet obtained by Squire [1].

If $Q_1 = Q_2 = Q$ and $B_1 = B_2 = B$, Equation (23) becomes the dispersion relation characterizing the instability of a plane power-law liquid jet into symmetric bounded gas medium:

$$\begin{aligned} & \frac{(S+im)^2}{L} \tanh(L) + Q \frac{S^2}{m} \coth[m(B - 1)] + \frac{m^2}{We} = 0 \\ & \frac{(S+im)^2}{L} \coth(L) + Q \frac{S^2}{m} \coth[m(B - 1)] + \frac{m^2}{We} = 0 \end{aligned} \tag{24}$$

When setting $B \rightarrow \infty$, Equation (24) is changed into the case of a power-law jet in an unbounded gas media, which is deduced by Xia et al. [20] as:

$$\begin{aligned} & \frac{(S+im)^2}{L} \tanh(L) + Q \frac{S^2}{m} + \frac{m^2}{We} = 0 \\ & \frac{(S+im)^2}{L} \coth(L) + Q \frac{S^2}{m} + \frac{m^2}{We} = 0 \end{aligned} \tag{25}$$

3. Results and Discussion

For every unstable curve between the growth rate S_r and the wave number m , there are three main unstable parameters, i.e., the dimensionless maximum growth rate $S_{r,max}$, the dimensionless dominant wave number m_{dom} , and the cutoff wave number m_c . Under a given flow condition, the three parameters are respectively characterizing the unstable degree, the primary breakup scale and the unstable range of liquid jets. In practice, the parameter G is gained by the comparison between the

theoretical prediction and the experiment results. In the current analysis, G is fixed at 2.5×10^{-6} to investigate the effect of two asymmetric gas media.

The breakup length of the plane power-law liquid jet is defined as the distance from the nozzle outlet to the point where ligament formation occurs along the symmetry axes of the plane [18]. According to the linear instability theory, the breakup length L_b of the jet is estimated by Heislbetz et al. [23] which can be expressed by:

$$L_b = u_l \ln(\eta_b/\eta_0)/s_{r,max} \quad (26)$$

where, $s_{r,max}$ represents the maximum growth rate gained by Equation (22), u_l the jet velocity, η_0 the initial disturbance amplitude, η_b the disturbance amplitude where breakup occurs and $\ln(\eta_b/\eta_0)$ a parameter related with the amplitude of interface waves. In the Equation (27) the initial disturbance wave amplitude is determined by the jet geometry and the flow conditions, and the liquid velocity u_l is given for different cases. However, η_b cannot be calculated by the linear analysis. Therefore, $\ln(\eta_b/\eta_0)$ cannot be obtained by the above analysis and is considered as an empirical constant. Researchers have made great efforts on this parameter, such as Deng [21], Weber [24], Dombrowski [25], Kroesser [26] and Kim [27]. Weber [24] pointed out that this parameter could be fixed at the value of 12 in their study range. Thus $\ln(\eta_b/\eta_0) = 12$ has been widely adopted [25]. Kroesser [26] gained a value of 11 for Newtonian liquid sheets. Nevertheless, with the development of technology, some investigators reported that the term of $\ln(\eta_b/\eta_0)$ is not a universal value and has to be determined experimentally in each case, such as Xia et al. [20] and Kim [27]. Besides, compared with the Newtonian liquid jet, the liquid viscosity of power-law fluids will vary with the liquid velocity, which may cause the parameter $\ln(\eta_b/\eta_0)$ to change.

In order to validate our work, the comparison between Deng's experiment data [21] and theoretical prediction curves are shown in Figure 2 in three cases, where (1) $\ln(\eta_b/\eta_0) = 12$; (2) $\ln(\eta_b/\eta_0) = 11$ and (3) $\ln(\eta_b/\eta_0)$ varies with the jet conditions. The other working parameters are fixed at $K = 28.1 \text{ Pa}\cdot\text{s}^n$, $n = 0.53$, $h = 0.0001 \text{ m}$, $\rho_l = 1000 \text{ kg m}^{-3}$, $\rho_{g1} = \rho_{g2} = 1.25 \text{ kg m}^{-3}$, $\sigma = 0.0732 \text{ N m}^{-1}$, $u_l = 26\text{--}36 \text{ m s}^{-1}$, $G = 2.5 \times 10^{-6}$. Here n is set to be smaller than 1, indicating that shear-thinning power-law fluid is used in the study.

It is found that the breakup length of theoretical results and experimental results are always in the same order, and their changing trends with jet velocity are also consistent when $\ln(\eta_b/\eta_0) = 11$ or 12. This shows that the current analysis results are reliable although there are some discrepancies mainly resulted from the nonlinear feature of power-law fluids and some simplification of viscosity terms. If $\ln(\eta_b/\eta_0)$ is considered as a correction coefficient of L_b and varies with u_l , the prediction curve 3 is obtained. It also demonstrates that, for power-law fluids, $\ln(\eta_b/\eta_0)$ varies with the jet velocity. This may be mainly resulted from the shear-thinning feature.

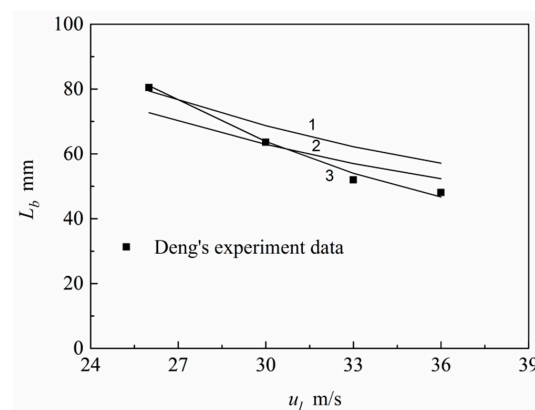


Figure 2. Comparison between Deng's experiment data and the prediction curves in terms of breakup length L_b as a function of jet velocity u_l . Lines 1–3 represent $\ln(\eta_b/\eta_0) = 12$, 11, and variable $\ln(\eta_b/\eta_0)$.

3.1. Effect of Gas Boundary Asymmetry

Figure 3 shows the effect of gas confinement on the instability of a plane power-law liquid jet in low-speed and high-speed cases.

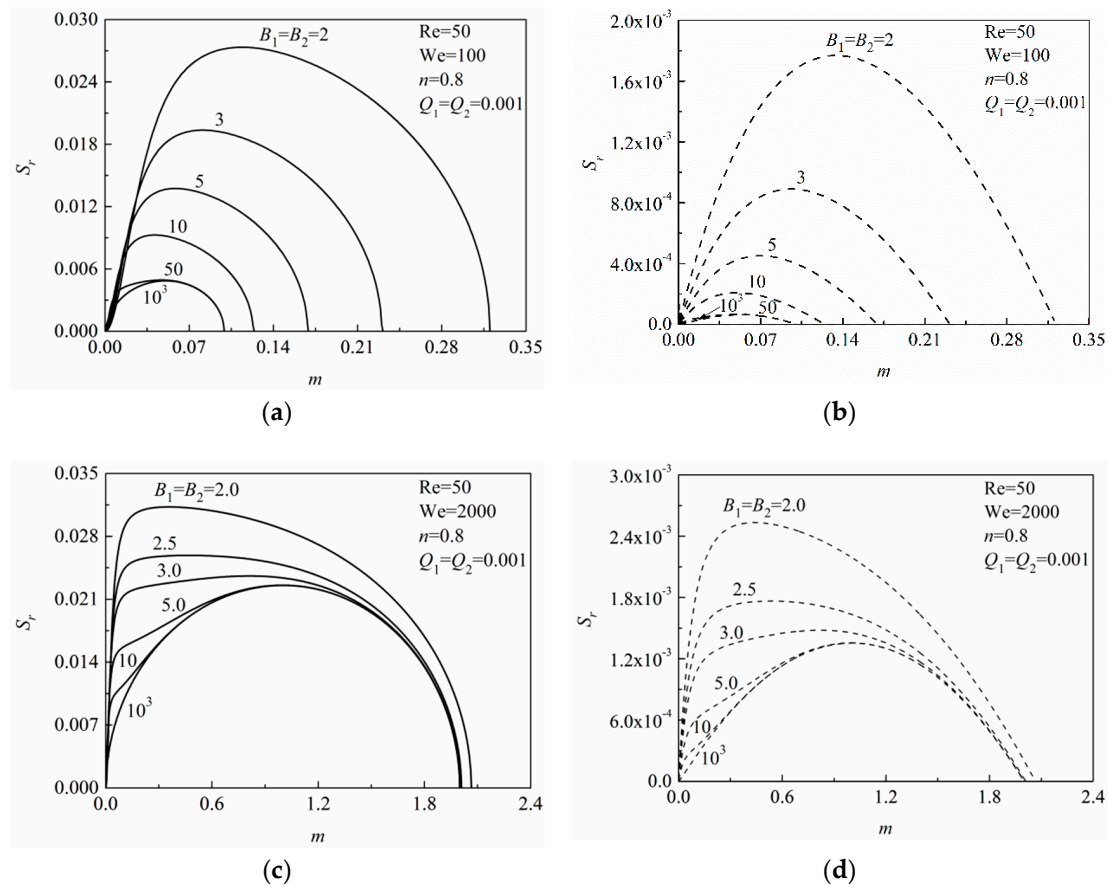


Figure 3. The dimensionless growth rate S_r of disturbance waves as a function of the non-dimensional wave number m for low (a,b) and high speed (c,d) jet. The solid (a,c) and dashed lines (b,d) represent para-sinusoidal mode and para-varicose mode respectively.

The parameters are fixed at $Re = 50$, $Q_1 = Q_2 = 0.001$, $n = 0.8$. The upper row is for low-speed jet ($We = 100$) case, and the lower row for high-speed jet ($We = 2000$) one. It should note that in order to ensure the existence of the gas media between the liquid phase and the solid wall, the distances b_1^* and b_2^* from gas boundaries of both sides to the x -axis must be larger than the half-thickness of the liquid h , i.e., $B_1 > 1$ and $B_2 > 1$. From Figure 3, it is found that, with the increase of B_1 and B_2 , the dimensionless maximum growth rate is decreased both for two jet cases and for two disturbances. The unstable range will be increased with a confined gas environment for both disturbances. This shows that a limited gas medium will promote the jet instability. The reasons are chiefly as follows. When $Q_1 = Q_2$ and $B_1 = B_2$, Equation (23) reduces to Equation (24), and the gas media on both sides of the liquid jet will become symmetrical. Furthermore, setting B going to infinite, the gas boundary will disappear and Equation (25) is gained. Compared with Equation (25), it is found that the second term of Equation (24) is the counterpart of Equation (25) multiplied by an additional term $\coth[m(B-1)]$. Note that the double cotangent function $\coth(x)$ is always larger than one when the independent variable x is larger than zero. When x tends to infinite, $\coth(x)$ tends to unit. This reveals that a limited gas medium will strengthen the relative motion between gas-liquid phases so as to promote the jet instability.

The physical mechanism is that the relative motion between gas molecules will become more intense in a limited gas space. This will cause more gas molecules to collide with gas-liquid interfaces at

unit time so as to promote the jet instability. However, with the increase of the Weber number, the effect of gas confinement is becoming less and less. The reason is that, with the increase of liquid velocity, the apparent viscosity of liquid phase will be reduced resulting from the shear-thinning feature and the aerodynamic force is enlarged constantly. Accordingly, in high-speed jet case, the interface instability is mainly controlled by the gas-liquid relative motion. In contrary, the gas confinement has a more noticeable effect on the jet instability in a relative low-speed jet case.

In order to investigate the asymmetric degree between two gas gaps on both sides of the liquid jet, a parameters B_c is defined as following, called as the boundary asymmetric degree:

$$B_c = \frac{b_1^*}{b_2^*} \tag{27}$$

Clearly, with a limited gas environment, i.e., $B_1 + B_2 = \text{constant}$, $B_c < 1$ represents that the gas thickness of left side is larger; otherwise $B_c > 1$ represents that the right side is larger. When $B_c = 1$, two gas thickness are the same.

Figure 4 shows the dimensionless growth rate S_r versus the wave number m under different We and the degree of gas boundary asymmetry. The low ($We = 100$) and high ($We = 2000$) Weber number cases denote low-speed and high-speed cases, respectively. The other parameters are fixed at $Re = 50$, $Q_1 = Q_2 = 0.001$, $B_1 + B_2 = 100$, $n = 0.8$. It is found that the liquid jet in unequal gaps is more unstable. In detail, with the asymmetric degree B_c increasing, the dimensionless maximum growth rate of two modes S_r for both low and high speed cases are amplified constantly.

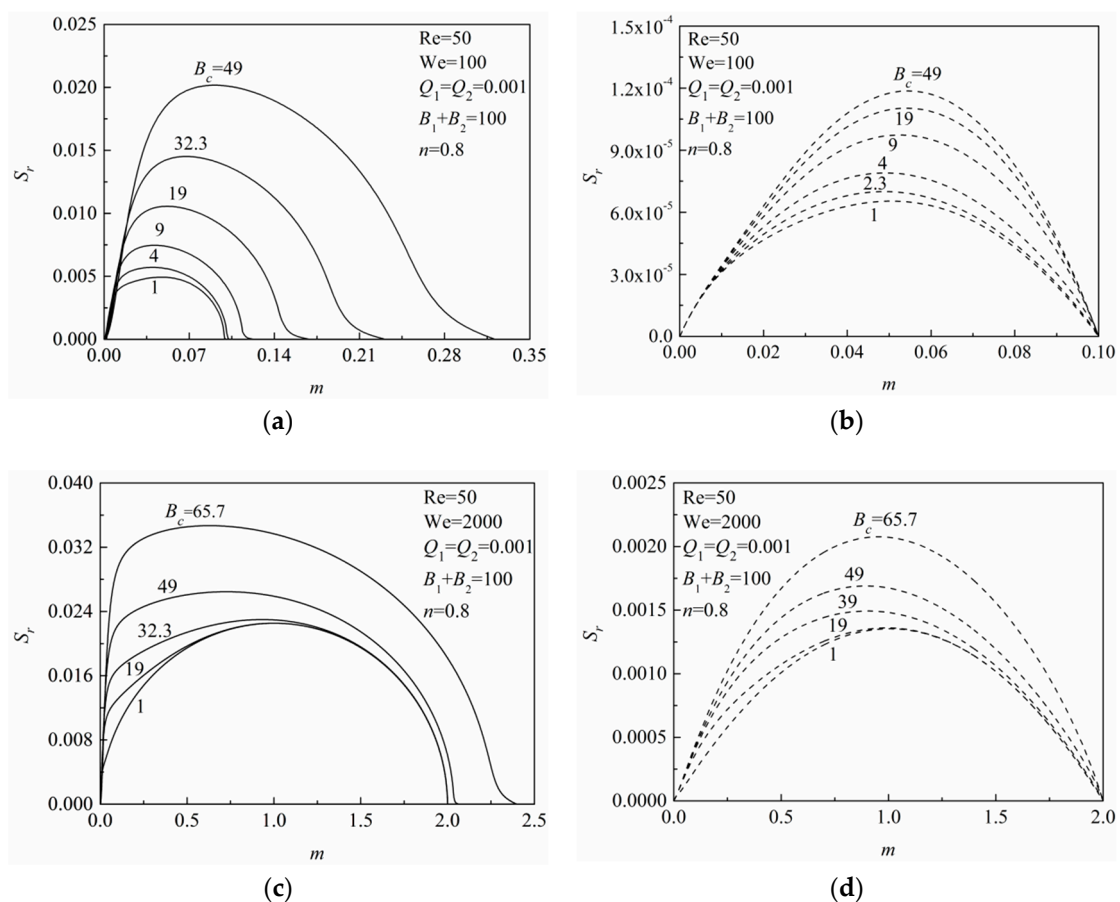


Figure 4. The dimensionless growth rate S_r of disturbance waves as a function of the non-dimensional wave number m on different We numbers: (a,b) $We = 100$ and (c,d) $We = 2000$. The solid and dashed lines represent para-sinusoidal mode and para-varicose mode respectively.

The unstable range of para-sinusoidal mode is increased while it remains nearly constant for the para-varicose mode. This indicates that the asymmetric gas medium has an unstable effect on the jet instability. The para-sinusoidal mode always prevails over para-varicose mode under different asymmetric boundary conditions, implying that the gas boundary asymmetry is beneficial for the disintegration of power-law fluids.

3.2. Effect of the Aerodynamic Asymmetry

In this section, two parameters Q_a and W are defined as follows to characterize the asymmetric degree of aerodynamic forces and the total perturbation energy of gas media on both sides of the jet respectively:

$$Q_a = \frac{\rho_{g1}(u_l - u_{g1})^2}{\rho_{g2}(u_l - u_{g2})^2} \quad W = \rho_{g1}(u_l - u_{g1})^2 + \rho_{g2}(u_l - u_{g2})^2 \quad (28)$$

Given that the gas media keeps still and the liquid velocity does not change, the two parameters are simplified to $Q_a = \rho_{g1}/\rho_{g2}$ and $W = (\rho_{g1} + \rho_{g2})u_l^2$. Therefore, when the sum of two gas density ratios $Q_1 + Q_2$ is fixed, the total perturbation energy remains the same. In addition, $Q_a > 1$ represents the perturbation energy in the right side of the liquid jet is larger than the left side, while $Q_a < 1$ means the right side is weaker. Accordingly, the perturbation energy on both sides become equal at the condition of $Q_a = 1$. In other words, the aerodynamic forces are distributed symmetrically. However, no matter the disturbance energy on the right or left side is stronger, the jet instability holds the line as long as the relative asymmetric degree between two gas densities $Q_d = |Q_1 - Q_2|$ is fixed.

As pointed out by Chang [22], the gas-liquid interaction force will become the leading factor to destabilize the liquid jet in high-speed cases. Figure 5 shows the effect of the aerodynamic asymmetry Q_a on the jet instability under a high speed flow condition. For $Re = 50$, $We = 1850$, $n = 0.8$, $B_1 = B_2 \rightarrow \infty$, it is found that with Q_a increasing from 1 to 100 or decreasing from 1 to 1/100, the dimensionless maximum growth rate $S_{r,max}$, the dimensionless dominant wave number m_{dom} and the unstable range of para-sinusoidal mode all increase. On the contrary, these three unstable parameters of para-varicose mode all decrease for increasing or decreasing Q_a from 1. When the total disturbance energy of two gas media on both sides of the liquid jet is equal ($Q_a = 1$), the $S_{r,max}$ of para-varicose mode reaches the peak, while the counterpart of para-sinusoidal mode decreases to the minimum. This reveals that the aerodynamic asymmetry will destabilize para-sinusoidal mode, while damper para-varicose mode.

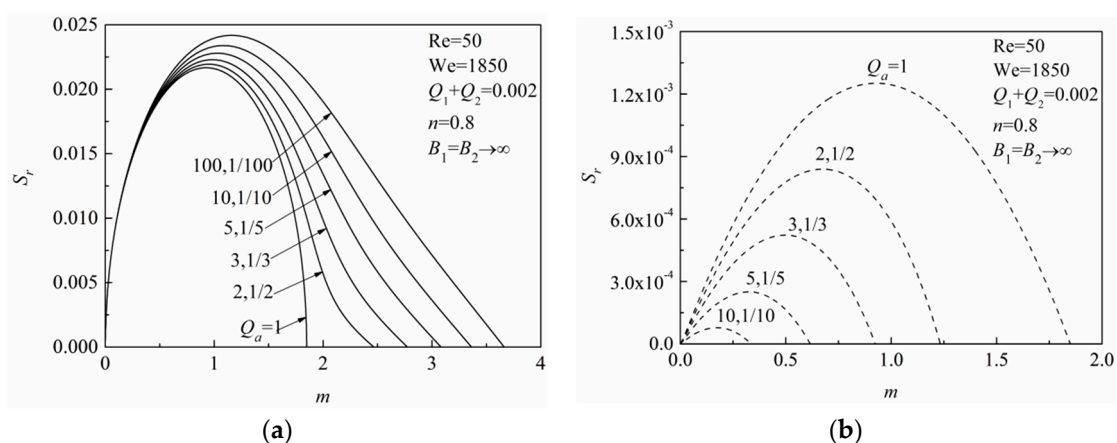


Figure 5. The dimensionless growth rate S_r of disturbance waves as a function of the non-dimensional wave number m for different asymmetric degree of aerodynamic forces Q_a : (a) para-sinusoidal mode (solid line); (b) para-varicose mode (dash line).

The reason is that when the total disturbance energy remains unchanged, one of the two aerodynamic forces will be enlarged while the other will be reduced with the change of Q_a .

Furthermore, two forms of interface waves have relationship with the aerodynamic forces on both sides. Para-sinuuous mode is related with the larger one while the smaller one is associated with para-varicose mode. Similar results were reported by Yang et al. [5]. Therefore, as the asymmetric degree of two aerodynamic forces increases, the opposite tendency of both disturbance modes is observed.

Besides, the maximum growth rate of para-sinuuous mode is larger than that of para-varicose mode. This indicates that para-sinuuous mode will dominate the jet breakup process and the aerodynamic asymmetry could effectively promote the breakup of power-law fluids. It is notable to see that the increasing rate of $S_{r, max}$ decreases with an increase of Q_a until approaching a certain limit in Figure 5.

Considering that para-sinuuous mode prevails over para-varicose mode in the jet breakup, Figure 6 will only show the maximum growth rate $S_{r, max}$ (a) and dominant wave number m_{dom} (b) with para-sinuuous mode for $Re = 50$, $We = 1850$, $n = 0.8$ and $B_1 = B_2 \rightarrow \infty$, to reveal the effect of total perturbation energy W on the jet instability.

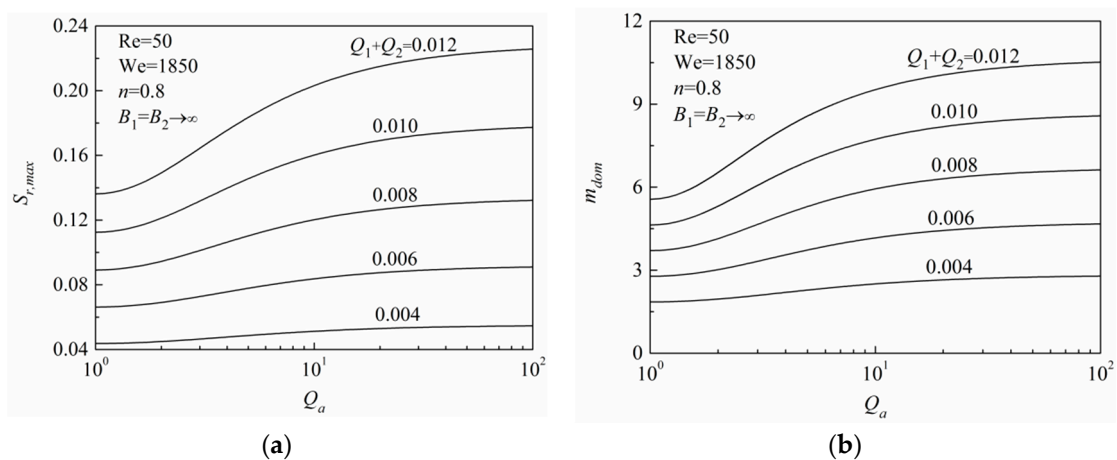


Figure 6. Effect of the aerodynamic asymmetry on jet instability at different total disturbance energy W with para-sinuuous mode: (a) dimensionless maximum growth rate; (b) dimensionless dominant wave number.

As the total disturbance energy of two gas media increases, $S_{r, max}$ and m_{dom} all increase significant accordingly. This indicates that with larger total gas disturbance energy, the aerodynamic asymmetry enables power-law fluids to break quickly smaller droplets. In other words, the aerodynamic asymmetry could dramatically accelerate the liquid breakup process in a high density gas media. Besides, compared with the boundary asymmetry, the aerodynamic asymmetry is much effective to trigger shorter interface waves. In practice applications, high-speed jets can be employed to achieve better mixing and combustion. As a result, the dominant interface waves are located at the short wave range. The aerodynamic asymmetry could be more effective to improve the atomization quality of liquid fuels.

Figure 7 presents the effect of the aerodynamic asymmetry on the jet instability at different Weber numbers, while other parameters are held at $Re = 50$, $n = 0.8$ and $B_1 = B_2 \rightarrow \infty$. This gives more information about the plane jet of power-law fluids in asymmetric gas media. It is found that with a fixed Weber number, both the dimensionless maximum growth rate and the dimensionless dominant wave number increase with the increase of Q_a . Specifically, this increasing trend becomes more significant with the increase of the Weber number constantly. This indicates that in the high-speed jet, the aerodynamic asymmetry could promote the breakup of power-law fluids more easily and also decrease the breakup scale. Thus, larger surface tensions or lower liquid velocities enable the plane jet of power-law fluids to become more stable in both asymmetric and symmetric cases.

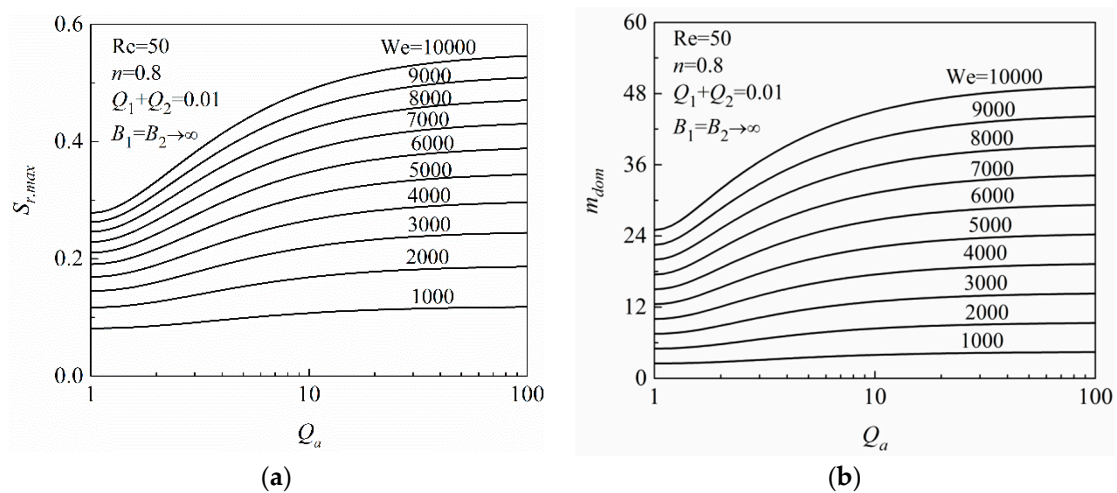


Figure 7. Effect of the aerodynamic asymmetry on jet instability at different Weber number with para-sinusous mode: (a) dimensionless maximum growth rate; (b) dimensionless dominate wave number.

3.3. Effect of Gas Asymmetric Distribution on the Unstable Range

The effect of the boundary asymmetric degree B_c on unstable range at $Q_1 = Q_2 = 0.001$, $n = 0.8$, and $B_1 + B_2 = 1000$ is presented in Figure 8. $B = 1$ represents the liquid fuel injecting into the symmetrical gas medium, then the cut-off wave numbers of para-sinusous and para-varicose modes are equivalent ($m_1 = m_2$). There exists a critical curve to distinguish the unstable regime with the stable regime. In Figure 8a, as B_c is increased from 1 to 500, the unstable range of para-sinusous mode is enlarged while para-varicose mode remains nearly constant as shown in Figure 8b. Additionally, with the increase of the Weber number, the difference among the cut-off numbers in terms of para-sinusous mode becomes smaller and smaller in Figure 8a. This indicates that the boundary asymmetry could enlarge the disturbance in a power-law plane jet but it plays a more significant role on low Weber number cases.

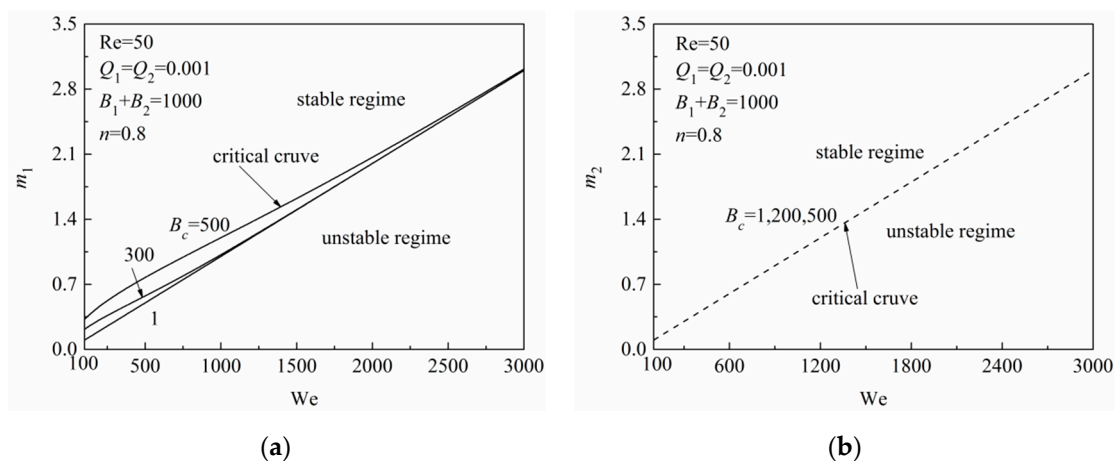


Figure 8. Effect of the boundary asymmetry on the unstable range of power-law plane jets: (a) para-sinusous mode (solid line); (b) para-varicose mode (dash line).

In order to explore the effect of the aerodynamic asymmetric degree Q_a on the unstable range of power-law plane jets, Q_a is set to increase from 1 to 1000. The results are shown in Figure 9, and the other parameters are $Q_1 + Q_2 = 0.002$, $n = 0.8$, and $B_1 = B_2 \rightarrow \infty$. If $Q_a = 1$, two gas media are symmetrical. It can be seen from Figure 9a,b that as the Weber number is increased from 100 to

10,000, the cut-off wave number of both disturbances (m_1, m_2) all increase. Higher Q_a leads to a larger unstable area of para-sinuuous mode, but a smaller unstable area of para-varicose mode instead. It is noted that para-sinuuous mode relates with the liquid breakup in this study. Therefore, an asymmetric gas environment will enhance the interface instability and result in short breakup lengths.

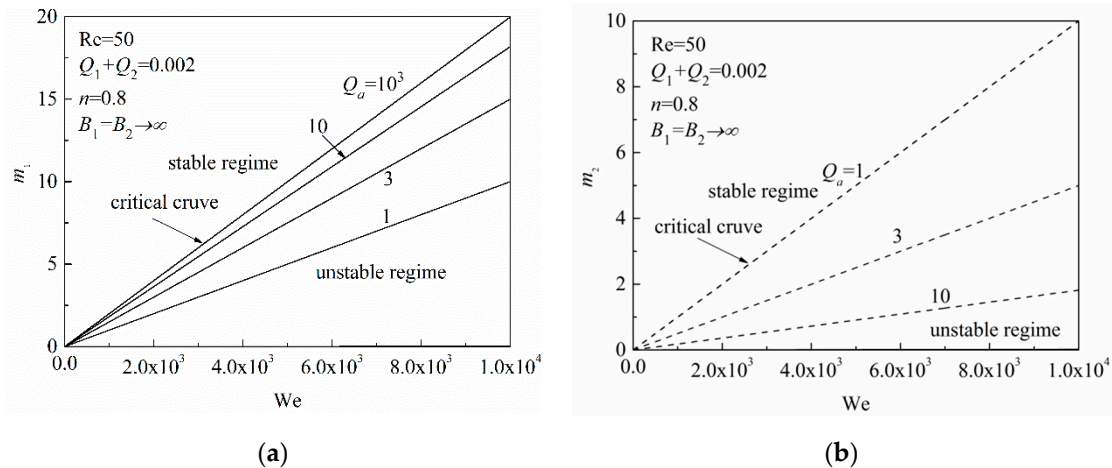


Figure 9. Effect of the aerodynamic asymmetry on the unstable range of power-law plane jets: (a) para-sinuuous mode (solid line); (b) para-varicose mode (dash line).

4. Conclusions

The instability characteristics of power-law fluids on a plane jet are investigated by a linear instability analysis in the presence of gas asymmetric distributions, including the boundary asymmetry and the aerodynamic asymmetry. It is found that a confined space will enhance the perturbation of gas medium on the jet instability. Under two kinds of gas asymmetric conditions, para-sinuuous mode always dominates the liquid breakup. Also, the gas asymmetric distribution could accelerate the disintegration of power-law fluids. With a large Weber number, the aerodynamic asymmetry is more useful to promote the liquid breakup than the boundary asymmetry. For a larger gas density and a higher liquid velocity, the promotion of the aerodynamic asymmetry will become more significant. In addition, the effects of two asymmetric distributions on the unstable range of power-law plane jets regarding to para-sinuuous and para-varicose disturbances are analyzed and the critical curves are obtained to characterize unstable and stable regimes. These conclusions are beneficial for better understanding of the breakup characteristic of power-law fluids in confined asymmetric gases.

Author Contributions: Data curation, J.-P.G.; Formal analysis, Y.-B.W. and Q.D.; Investigation, J.-P.G. and Y.-B.W.; Methodology, F.-Q.B. and Q.D.; Resources, F.-Q.B., F.Z. and Q.D.; Writing—original draft, Y.-B.W.; Writing—review & editing, J.-P.G., F.Z. and Q.D.

Funding: This research was funded by [National Natural Science Foundation of China] grant number [51676135] and [Tianjin Research Program of Application Foundation and Advanced Technology] grant number [15JCZDJC39600].

Conflicts of Interest: The authors declare no conflict of interest.

Nomenclature

h	half-thickness of the liquid jet
a^*	gas boundary
ρ	density
i	$(-1)^{0.5}$
k	wave number
B	dimensionless gas boundary, b_j^*/h
Q	gas-liquid density ratio

B_c	asymmetric degree of gas boundaries on both sides
Q_a	asymmetric degree of aerodynamic forces on both sides
m	kh
n	power law exponent
K	consistency coefficient
Re	Generalized Reynolds number of liquid phase, $\rho_l u_l^{2-n} h^n / K$
L	$[1 + 2n(2G)^{n-1} m^2 \text{Re}^{-1} (S + im)^{-1}]^{-0.5} m$
t	time
p	pressure perturbation
u	velocity perturbation vector
u_l	liquid jet velocity
x	coordinate parallel to the liquid jet
y	coordinate normal to the liquid jet
η	interface displacement from the balance position
η_0	initial disturbance amplitude
η_b	disturbance amplitude where breakup occurs
We	liquid Weber number, $\rho_l u_l^2 h / \sigma$
σ	surface tension
S	sh / u_l
s	complex growth rate
Subscripts	
j	$l, 1$ or 2
l	liquid phase
$1, 2$	right or left gas media

References

1. Squire, H.B. Investigation of the instability of a Moving Liquid Film. *Br. J. Appl. Phys.* **1953**, *167*, 167–169. [[CrossRef](#)]
2. Li, X.; Tankin, R.S. On the Temporal Instability of a Two-Dimensional Viscous Liquid Sheet. *J. Fluid Mech.* **1991**, *226*, 425–443. [[CrossRef](#)]
3. Li, X. Spatial Instability of Planar Liquid Sheets. *Chem. Eng. Sci.* **1993**, *148*, 2973–2981. [[CrossRef](#)]
4. Cao, J.M.; Li, X. Stability of Plane Liquid Sheets in compressible Gas Streams. *J. Propul. Power* **2000**, *16*, 623–627. [[CrossRef](#)]
5. Jazayeri, S.A.; Li, X. Nonlinear instability of plane liquid sheets. *J. Fluid Mech.* **2000**, *406*, 281–308. [[CrossRef](#)]
6. Ibrahim, E.A.; Marshall, S.O. Instability of a Liquid jet of Parabolic Velocity Profile. *Chem. Eng. J.* **2000**, *76*, 17–21. [[CrossRef](#)]
7. Negeed, E.R.; Hidaka, S.; Heitoyr, M.V. Liquid Film Disintegration Regimes and Proposed Correlations. *Int. J. Multiph. Flow* **2002**, *28*, 773–789.
8. Zhao, H.; Liu, H.F.; Xu, J.L.; Li, W.F. Secondary breakup of coal water slurry drops. *Phys. Fluids* **2011**, *23*, 074501. [[CrossRef](#)]
9. Yang, L.J.; Du, M.L.; Fu, Q.F.; Tong, M.X.; Wang, C. Temporal instability of a power-law plane Liquid Sheet. *J. Propul. Power* **2015**, *31*, 286–293. [[CrossRef](#)]
10. Liu, Z.; Brenn, G.; Durst, F. Linear analysis of the instability of two-dimensional non-Newtonian liquid sheets. *J. Non-Newton. Fluid Mech.* **1998**, *78*, 133–166. [[CrossRef](#)]
11. Brenn, G.; Liu, Z.; Durst, F. Three-dimensional temporal instability of non-Newtonian liquid sheets. *Atomization Sprays* **2001**, *11*, 49–84. [[CrossRef](#)]
12. Yang, L.J.; Xu, B.R.; Fu, Q.F. Linear instability of planar non-Newtonian liquid sheets in two gas streams of unequal velocities. *J. Non-Newton. Fluid Mech.* **2012**, *167–168*, 50–58. [[CrossRef](#)]
13. Fu, Q.; Yang, L.; Chen, P.; Liu, Y.; Wang, C. Spatial-Temporal Stability of an Electrified Viscoelastic Liquid Jet. *ASME J. Fluids Eng.* **2013**, *135*, 094501. [[CrossRef](#)]
14. Thompson, J.C.; Rothstein, J.P. The atomization of viscoelastic fluids in flat-fan and hollow-cone spray nozzles. *J. Non-Newton. Fluid Mech.* **2007**, *147*, 11–22. [[CrossRef](#)]

15. Liu, L.J.; Lu, L.P. Instability of Viscoelastic Annular Liquid Jets in a Radial Electric Field. *ASME J. Fluids Eng.* **2014**, *136*, 081202. [[CrossRef](#)]
16. Chojnacki, K.T.; Feikema, D.A. Study of non-Newtonian Liquid Sheets Formed by impinging Jets. In Proceedings of the 33rd Joint Propulsion Conference and Exhibit, Seattle, WA, USA, 6–9 July 1997; p. 3335.
17. Yang, L.J.; Fu, Q.F.; Qu, Y.Y.; Gu, B.; Zhang, M.Z. Breakup of a power-law liquid sheet formed by an impinging jet injector. *Int. J. Multiph. Flow* **2012**, *39*, 37–44. [[CrossRef](#)]
18. Ma, Y.C.; Bai, F.Q.; Chang, Q.; Yi, J.M.; Jiao, K.; Du, Q. An experimental study on the atomization characteristics of impinging jets of power law fluid. *J. Non-Newton. Fluid Mech.* **2015**, *217*, 49–57. [[CrossRef](#)]
19. Huang, C.C.; Chen, J.L.; Wang, J.S. Linear Stability of Power Law Liquid Films Down an Inclined Planar. *J. Phys. D Appl. Phys.* **1994**, *27*, 2297–2301.
20. Xu, L.X.; Xia, Z.Y.; Zhang, M.Z.; Du, Q.; Bai, F.Q. Experimental research on breakup of 2D power law liquid film. *Chin. J. Chem. Eng.* **2015**, *23*, 1429–1439. [[CrossRef](#)]
21. Deng, H.Y.; Feng, F.; Wu, X.S. Dual-mode linear analysis of temporal instability for power-law liquid sheet. *Atomization Sprays* **2016**, *26*, 319–347. [[CrossRef](#)]
22. Chang, Q.; Zhang, M.Z.; Bai, F.Q.; Wu, J.P.; Xia, Z.Y.; Jiao, K.; Du, Q. Instability analysis of a power law liquid jet. *J. Non-Newton. Fluid Mech.* **2013**, *198*, 10–17. [[CrossRef](#)]
23. Heislbetz, B.; Madlener, K.; Ciezki, H. Breakup characteristics of a Newtonian liquid sheet formed by a doublet impinging jet injector. In Proceedings of the 43rd AIAA/ASME/SAE/ASEE Joint Propulsion Conference & Exhibit, Cincinnati, OH, USA, 8–11 July 2007; p. 5694.
24. Weber, C. Disintegration of liquid jets. *J. Appl. Math. Mech.* **1931**, *11*, 136–159.
25. Dombrowski, N.; Hooper, P.C. The effect of ambient density on drop formation in sprays. *Chem. Eng. Sci.* **1962**, *17*, 291–305. [[CrossRef](#)]
26. Kroesser, F.W.; Middleman, S. Viscoelastic jet instability. *AIChE J.* **1969**, *15*, 383–386. [[CrossRef](#)]
27. Kim, D.J.; Im, J.H.; Yoon, Y.B. Effect of ambient gas density on spray characteristics of swirling liquid sheets. *J. Propul. Power* **2007**, *23*, 603–611. [[CrossRef](#)]



© 2018 by the authors. Licensee MDPI, Basel, Switzerland. This article is an open access article distributed under the terms and conditions of the Creative Commons Attribution (CC BY) license (<http://creativecommons.org/licenses/by/4.0/>).